Applied Catalysis B: Environmental 117–118 (2012) 253–259

Contents lists available at SciVerse ScienceDirect

Applied Catalysis B: Environmental

journal homepage: www.elsevier.com/locate/apcatb

Hydrogenolysis of glycerol to obtain 1,2-propanediol on Ce-promoted Ni/SBA-15 catalysts

I. Jiménez-Morales [a], F. Vila [b], R. Mariscal [b], A. Jiménez-López [a,*]

[a] Departamento de Química Inorgánica, Cristalografía y Mineralogía (Unidad Asociada al ICP-CSIC), Facultad de Ciencias, Universidad de Málaga, Campus de Teatinos, 29071 Málaga, Spain
[b] Group of Sustainable Energy and Chemistry (EQS), Institute of Catalysis and Petrochemistry (ICP-CSIC), C/Marie Curie 2, Cantoblanco, 28049 Madrid, Spain

ARTICLE INFO

Article history:
Received 22 November 2011
Received in revised form 18 January 2012
Accepted 21 January 2012
Available online 30 January 2012

Keywords:
Glycerol
Hydrogenolysis
SBA-15
Acid catalysts
Metallic nickel
Ceria

ABSTRACT

Metallic Ni (10 wt.%) supported on SBA-15 silica and promoted with cerium loading ranged between 2.5 and 10 wt.%, reduced at 723 K during 1 h, were used as catalysts in the hydrogenolysis of a glycerol aqueous solution (80 wt.%) at 473 K and 2.4 MPa of H_2 pressure. Whereas pure Ni catalyst mainly produces volatile products by C—C hydrogenolysis reaction, the promoted cerium catalysts lead to the formation of 1,2-propanediol (1,2-PDO) as majority product. After 8 h of reaction the catalyst with 10 wt.% of Ni and 7.5 wt.% of Ce gives the maximum glycerol conversion and selectivity to 1,2-PDO, with yield of this substance of 24.2%/g of catalyst. The presence of cerium species is essential to produce 1,2-PDO. The effect of cerium oxide is to act as strong acid sites (TPD-NH_3), improve the metallic Ni dispersion (XRD, H_2 chemisorption and XPS) and to make more difficult their reduction (TPR). The stronger acidity suggests that the formation of acetol takes place easier in these catalysts and subsequently this intermediate is reduced by activated hydrogen from the nearby Ni metallic sites.

1. Introduction

Biodiesel is defined as a mixing of methyl esters of light alcohols such as methanol and ethanol derived from fatty acids obtained from renewable sources such as vegetable oils and animal fats. Most biodiesel is currently produced by transesterification of these triglycerides with methanol in the presence of homogeneous basic catalysts. The principal by-product of biodiesel production and soap industries is the crude glycerol. The rapid development of biodiesel production formed large quantities of this product. For every 9 kg of biodiesel produced, about 1 kg of glycerol is obtained. The recovery of high quality glycerol as a biodiesel by-product is the primary option to be considered to lower the cost of biodiesel; but if it is used in food, cosmetics and drugs, further purifications are needed [1]. Purifying it to that level is costly and generally out of the range of economic feasibility for the small to medium sized plants.

Glycerol is a building block that plays an important role in biorefinery as a feedstock [2,3]. Thus, it can be converted in hydrogen and synthesis gas by a reforming reaction [4,5]. One method of interest is the conversion of glycerol through a hydrogenolysis reaction to oxygenated petrochemicals such as propanediols [6,7], acrolein [8,9] and glyceric acid [10]. This is an important example to obtain these commodity products not only cheaper than the petroleum routes but also from renewable feedstocks. Ethylene and propylene glycol are industrially important chemicals used in the preparation of polymers, resins, antifreeze, foods and cosmetics.

Among the different possible transformations of glycerol, the selective conversion to 1,2-PDO and 1,3-PDO presents a special interest. The challenge of the recent research in hydrogenolysis of glycerol is the development of heterogeneous catalysts to carry out this reaction specifically, i.e. catalysts able to produce the cleavage by hydrogen of a C—OH bond preserving the C—C bonds from the glycerol molecules. The 1,3-propanediol is more valuable than 1,2-propanediol, and recently it is receiving a lot of attention and good results have been obtained by using noble metal supported catalysts [11–13] promoted by rhenium oxide. The catalytic hydrogenolysis of glycerol to 1,2-PDO has also attracted much attention in the recent years. Several transition metals have been studied as catalysts on this reaction, however high selectivity toward 1,2-PDO is not always achieved [5,14–16]. However, Ru supported on activated carbon in combination with Amberlyst [17–19] exhibits high activity in mild conditions. The influence of the support and catalyst reduction temperature on the catalytic performance in the hydrogenolysis of glycerol has been studied by Feng et al. [20]. Although several articles have been reported using Ru as active phase in this reaction [21], unfortunately this metal promotes excessive cleavage of C—C bonds resulting in a high selectivity to methane [22,23]. Pt, Cu as well as bimetallic catalysts such as Pt–Ru, Au–Ru and Ru–Re [24–27] have also been assayed in this reaction.

* Corresponding author. Tel.: +34 952131876; fax: +34 952137534.
E-mail address: ajimenezl@uma.es (A. Jiménez-López).

0926-3373/$ – see front matter © 2012 Elsevier B.V. All rights reserved.
doi:10.1016/j.apcatb.2012.01.027

Nickel is another transition element recently used as catalyst in this reaction. This element was been employed as Raney Nickel [28] or dispersed on different supports. The glycerol hydrogenolysis mechanism to obtain 1,2-PDO is broadly accepted that proceeds via dehydration to acetol on acid sites and a consecutive hydrogenation over metallic centers [18,29], consequently this reaction requires bifunctional catalysts. Zeolites [30], silica–alumina [31,32], and alumina [33] have been used as acid supports. A promoting effect was observed when nickel supported on activated carbon catalyst was promoted with cerium [34,35], owing to the cerium species can served as Lewis acid sites [36].

This paper deals with the preparation and characterization of Ni and Ce promoted Ni catalyst supported on a non acidic SBA-15 mesoporous silica, with high surface area, with the purpose to obtain highly dispersed active phases and their application to the hydrogenolysis of glycerol to get some insights into the role of cerium in the activity and selectivity of the reaction. The catalysts with different cerium contents were fully characterized by XRD, H_2-TPR, XPS, hydrogen chemisorption, nitrogen adsorption at 77 K and NH_3-TPD.

2. Experimental

2.1. Catalysts preparation

The support used in this work is low cost SBA-15 silica, which was prepared according to the method described elsewhere [37] by using sodium silicate as source of Si. This support was previously calcined at 823 K during 5 h. All samples were impregnated by the incipient wetness method with 10 wt.% of nickel employing an aqueous solution of nickel citrate. This solution was prepared by mixing nickel acetate and citric acid in a 2:3 molar ratio and heating at moderate temperature until the solution turned a bright-green color. It is well-known that the chelated nickel species formed with citric acid lead to a wetted and highly viscous film on the surface of the support giving rise to the formation of very small metallic particles after calcination and reduction [38,39]. Cerium was incorporated in the catalysts by simultaneous impregnation with nickel using $Ce(NO_3)_3{\cdot}6H_2O$ in amounts to get loadings ranged between 2.5 and 10 wt.% of Ce. All samples were dried at 333 K and then calcined at 823 K for 4 h. The samples were labelled as *X*Ce-Ni-SBA where *X* represents the Ce percentage.

2.2. Characterization techniques

Laboratory X-ray powder diffraction (XRPD) patterns were collected on a PAN analytical X'Pert Pro automated diffractometer. Powder patterns were recorded in Bragg–Brentano reflection configuration by using a Ge (1 1 1) primary monochromator (Cu $K\alpha_1$) and the X'Celerator detector with a step size of 0.017° (2θ). The powder patterns were recorded between 8° and 70° in 2θ with an equivalent counting time of 712 s/step.

X-ray photoelectron spectra were collected using a Physical Electronics PHI 5700 spectrometer with non-monochromatic Al Kα radiation (300 W, 15 kV, 1486.6 eV) with a multi-channel detector. Spectra of samples were recorded in the constant pass energy mode at 29.35 eV, using a 720 μm diameter analysis area. Binding energies were determined under an accuracy of ±0.1 eV. Charge referencing was measured against adventitious carbon (C 1s at 284.8 eV). A PHI ACCESS ESCA-V6.0 F software package was used for acquisition and data analysis. A Shirley-type background was subtracted from the signals. All recorded spectra were always fitted using Gaussian–Lorentzian curves to more accurately determine the binding energy of the different element core levels.

Temperature programmed reduction (H_2-TPR) experiments were carried out between 313 and 972 K, using a flow of Ar/H_2 (40 $cm^3\ min^{-1}$, 10 vol.% of H_2) and a heating rate of 10 K min^{-1}. The effluent gas was passed through a cold trap (193 K) before the thermal conductivity detector to remove water from the exit stream.

The textural parameters of the catalysts were evaluated from nitrogen adsorption–desorption isotherms at 77 K, as determined by an automatic ASAP 2020 system from Micromeritics, after degassing at 473 K and 1.3×10^{-2} Pa overnight.

Hydrogen chemisorption was performed in a Micromeritics ASAP 2010 apparatus, after in situ reduction of the samples at 723 K (15 K min^{-1}) for 1 h, under a flow of H_2. After reduction, the catalysts were degassed at 10^{-4} Pa for 10 h at the same temperature and cooled at 308 K to carry out the H_2 chemisorption. The range of pressures studied was 0.013–0.04 MPa, and the amounts of H_2 chemisorbed were calculated by extrapolation of the isotherms to zero pressure. Dispersion data have calculated assuming the stoichiometry H/Ni = 1. The average particle size was determined by using the following expression: $d = 431/S_m$ ($m^2\ g_{Ni}^{-1}$) nm [40]. The degree of reduction of nickel (α) was determined by oxygen chemisorption in the same apparatus. The samples were reduced and degassed in the same conditions, the oxygen chemisorption was carried out at 673 K, and the range of pressures studied was 0.013–0.08 MPa. In the determination of the degree of reduction of nickel was taken into account the amount of oxygen consumed by Ce^{3+} present in the samples as determined by XPS analysis.

The acidic properties of the catalysts were analyzed by the temperature-programmed desorption of ammonia (NH_3-TPD), previously adsorbed at 373 K, was carried out from room temperature to 823 K, with a heating rate of 10 K min^{-1} and maintaining the sample at 823 K for 15 min. The evolved ammonia was analyzed by online gas chromatography (Shimadzu GC-14A) provided with a TCD. Catalysts were pre-treated at atmospheric pressure by flowing helium (35 mL min^{-1}) from room temperature to 823 K with a heating rate of 10 K min^{-1} and maintaining the sample at 823 K for 1 h. Samples were cooled until 373 K under a helium flow and then ammonia was adsorbed at this temperature.

2.3. Catalytic activity measurements

Glycerol hydrogenolysis reactions were carried out in a glass-lined stainless steel autoclave Parr reactor with 100 mL capacity. Before reaction, catalysts were reduced at 723 K during 1 h under a flow 60 mL min^{-1} of H_2/Ar (5% v/v). In a typical experiment, 25 g of aqueous glycerol solution (80 wt.% glycerol, 20 wt.% H_2O) and 0.6 g of catalyst (3.0 wt.% with respect to glycerol) were loaded in the autoclave, which was then flushed several times with N_2 to remove the ambient air, the mixture was heated up to 473 K and stirring vigorously (500 rpm). Subsequently, the system was pressurized with H_2 till 3.0 MPa (kept unchanged during the entire duration of the reaction). After 8 h of reaction, the system was cooled down to room temperature. Reactants and products in the liquid were analyzed by gas chromatography (Agilent 6890 N) using a capillary column (ZB-WAX: 30 m × 0.32 mm × 0.50 μm) connected to a flame ionization detector (FID). The samples for chromatographic analysis were prepared by adding a certain amount of acetone (solvent) and ethyl valerate (internal standard) to 0.2 g of the liquid sample. Conversion was calculated as the molar ratio of the disappeared glycerol to the initial added. Selectivity is defined as the molar ratio of each product to the glycerol consumed in the reaction.

3. Results and discussion

3.1. Characterization of catalysts

Phase identification was realized by XRD patterns of CeNi reduced catalysts, prepared under the experimental conditions

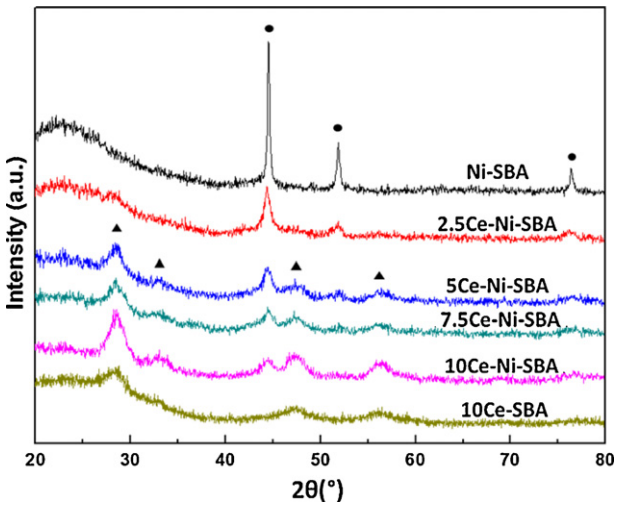

Fig. 1. XRD diffraction patterns of *X*Ce-Ni-SBA reduced catalysts, where 10Ce-SBA calcined catalyst was also included as reference. (●) metallic nickel, and (▲) CeO_2.

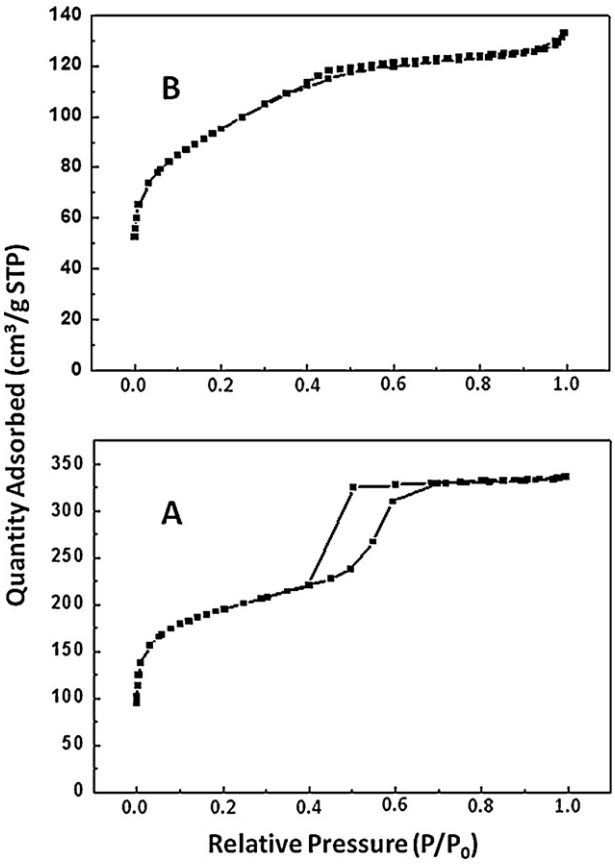

Fig. 2. N_2 adsorption isotherms at 77 K on (A) SBA-15 support and (B) 10Ce-Ni-SBA catalyst.

above indicated, i.e. reduced at 723 K during 1 h and under 60 mL min^{-1} of H_2/Ar (5% v/v). The diffractograms of these catalysts are compiled in Fig. 1. The diffraction pattern of Ni-SBA catalyst exhibits a set of peaks at 44.5, 51.8 and 76.4° characteristic of metallic nickel, JCPDS database (No. 01-1258). When cerium is incorporated in increasing amounts in the catalysts these peaks are enlarged and their intensities are clearly reduced indicating a higher dispersion of the metallic phase. In fact, the crystalline size of Ni^0 phase decreases from 4.9 nm for Ni-SBA catalyst till 0.7 nm for 10Ce-Ni-SBA, as determined by Scherrer equation and the diffraction peak at 44.5°. All the diffraction patterns of CeNi reduced catalysts show moreover the characteristic reflections of CeO_2 at 28.5, 33.4, 47.5 and 56.4°, which match well with the peaks of the cubic phase of the fluorite crystal structure in JCPDS database (No. 43-1002). In all cases the crystalline size of CeO_2 phase is very similar since they ranged from 1.0 nm until 1.3 nm, as determined by Scherrer equation and the diffraction peak at 28.5°. After the incorporation of Ce and Ni and to apply the reduction process all the catalysts maintain the mesoporous structure of the SBA-15 support since XRD patterns at low angles show a broad and intense peak centered at $2\theta = 1.1°$, similar to the pristine SBA-15 support (not shown here).

Textural characteristics were evaluated from nitrogen adsorption–desorption isotherms at 77 K. Whereas the pristine support exhibits reversible type IV isotherms in the IUPAC classification, with a sharp inflexion point at $P/P_0 = 0.35–0.40$, characteristic of capillary condensation within uniform mesopores with constant cross section and with a clear hysteresis loop of H1 type, the isotherms of catalysts appear modified after the incorporation of the active phases, although all them still present strong adsorption at medium relative pressures (Fig. 2). The surface area of Ni-SBA catalyst is lower than that of the pristine support (Table 1), due to the blockage of some pores by the Ni^0 particles. However the surface area of 2.5Ce-Ni-SBA is higher as a consequence of the better dispersion and lower particle size of nickel in this sample. For the other catalysts containing higher loadings of cerium, the BET specific surface areas and the accumulated pore volumes generally decrease as the cerium dioxide content rises (Table 1); thus, the higher reduction of BET area with respect to the pristine support was found for 10Ce-Ni-SBA. In general, all materials retain their mesoporous character and high surface areas after impregnation with Ni or CeNi.

The precursor catalysts were studied by H_2-TPR to evaluate the reducibility of nickel and cerium species. The Ni-SBA precursor exhibits an intense peak of H_2 consumption centered at 608 K (Fig. 3), corresponding to the reduction of well dispersed NiO on the silica support to Ni^0. However, a small band centered at higher temperatures (813 K) indicates the presence of NiO crystallites strongly interacting with the wall of mesopores and/or Ni^{2+} ions interacting with SiO^- groups [34]. As a reference the H_2-TPR analysis of a sample containing 10 wt.% of cerium supported on SBA-15, calcined at 823 K during 4 h, was also studied (Fig. 3). The profile of this sample only presents a very broad peak starting at 673 K and centered at about 773 K that accounts for a reduction of cerium atoms from CeO_2 to Ce_2O_3. When cerium is incorporated to the nickel catalyst,

Table 1
Textural propreties (N_2 isotherms) and surface acidity (NH_3-TPD) of support and CeNi reduced catalysts.

Catalyst	S_{BET} ($m^2 g^{-1}$)	V_p ($cm^3 g^{-1}$)	d_p (Å)	Acidity (μmol NH_3 g^{-1})	Acidity 300–550 °C (μmol NH_3 g^{-1})
SBA-15	675	0.39	23.1	64	–
Ni-SBA	481	0.29	24.1	830	430
2.5Ce-Ni-SBA	592	0.33	22.2	956	534
5Ce-Ni-SBA	431	0.25	23.2	1097	644
7.5Ce-Ni-SBA	354	0.20	26.2	1175	762
10Ce-Ni-SBA	336	0.21	25.0	1067	609

Table 2
Metallic characteristics of Ni deduced from H_2 chemisorption experiments of CeNi reduced catalysts.

Catalyst	Degree of reduction, α (%)	Dispersion, D (%)	Metallic area, S_m ($m^2\ g^{-1}$)	Metallic area, S_m ($m^2\ g_{Ni}^{-1}$)	Average particle size, d (nm)
Ni-SBA	14.9	13.2	1.3	88.0	4.9
2.5Ce-Ni-SBA	14.0	32.9	3.1	219.4	2.0
5Ce-Ni-SBA	12.1	47.8	3.9	319.1	1.4
7.5Ce-Ni-SBA	10.7	67.8	4.8	452.2	0.9
10Ce-Ni-SBA	12.8	60.9	5.2	406.2	1.1

the low temperature peak corresponding to the reduction of nickel is broadened indicating the existence of two components. That reveals the existence of two kinds of NiO in the samples, the first one is NiO interacting with the support as in the case of Ni-SBA material, while the second is NiO strongly interacting with the CeO_2 particles, appearing close to 648 K. Moreover, the intensity of the second peak is higher when the cerium loading increased, in such a way that the sample 10Ce-Ni-SBA exhibits a unique peak at 648 K, clearly indicating that all the nickel oxide species are interacting with the ceria particles. Finally, in all cases hydrogen consumption at high temperature (773–813 K) is also observed, due to the simultaneous superficial reduction of CeO_2 particles and NiO crystallites located in mesopores and/or Ni^{2+} ions neutralizing SiO^- groups [34].

The H_2 chemisorption on the catalysts data confirmed the above results. The corresponding data are gathered in Table 2. The low degree of reduction is consistent with a strong interaction of Ni^{2+} ions with the support and the ceria particles, and the reducibility of these ions is more difficult with the presence of increased amounts of ceria. As a consequence, the nickel dispersion greatly increases with the incorporation of cerium due to the interaction of NiO particles with ceria ones. In similar way, the metallic surfaces became higher across the group of catalysts attaining the maximum value for 7.5Ce-Ni-SBA catalyst. The metallic sizes of nickel determined by this technique match very well with those found by the Scherrer method, ranging from 4.9 and 0.9 nm.

To get insights on the chemical states of the elements of the active phases and their relative abundance at the catalyst surface, XPS analysis was run out of nickel and CeNi reduced catalysts. It is known that the core level Ce 3d signal of CeO_2 is composed of six peaks [41]: υ_0, υ_1, and υ_2 from Ce $3d_{5/2}$ and corresponding doublets υ'_0, υ'_1 and υ'_2 from Ce $3d_{3/2}$. The doublet υ_0/υ'_0 is originated from the final state Ce(IV) $3d^9\ 4f^2\ O2p^4$; the doublet υ_1/υ'_1 from the final state Ce(IV) $3d^9\ 4f^1\ O2p^5$ and finally the doublet υ_2/υ'_2 corresponds to final state Ce(IV) $3d^9\ 4f^0\ O2p^6$. Ce^{3+} species present a doublet υ_0/υ'_0 assigned to the final state Ce(III) $3d^9\ 4f^1\ O2p^6$ and another doublet υ_1/υ'_1 originated from the final state Ce(III) $3d^9\ 4f^2\ O2p^5$. When both oxidation states are present, the concentration of Ce(III) can be determined from the following equation: [Ce(III)] = [Ce(III)]/[Ce(III)] + [Ce(IV)], where the notations [Ce(III)] and [Ce(IV)] represent the corresponding sums of the integrated peaks areas related to the doublets of each oxidation state.

Fig. 4 shows the spectrum of calcined 7.5Ce-Ni-SBA and of CeNi reduced catalysts in the core level region of Ce 3d. Table 3 gathers the B.E. values of all peaks corresponding to all reduced catalysts and calcined 7.5Ce-Ni-SBA sample, which is included as reference. The spectrum of this solid can be deconvoluted into 10 peaks corresponding to Ce(IV) and Ce(III) species. The percentage of Ce(III) in this sample is only 9.9%, which can be due to the loss of O_2 under high vacuum, as has been reported in literature [37], in spite of the time of data acquisition was only 30 min. The spectra of CeNi reduced catalysts exhibit the same peaks, but those corresponding to Ce(III) are now more intense due to reduction process. The degree of reduction depends on the cerium loading. When the cerium content ranges between 2.5 wt.% and 7.5 wt.% the degree of reduction is around 35%, however for the highest cerium loading (10 wt.%) this value is only 27.4%. This result was expected since the reduction of CeO_2 particles could mainly take place on their surface; thus the 10Ce-Ni-SBA catalyst with bigger particles and, on the other hand, interacting with Ni particles, is reduced in a low extend [42].

Regarding the XPS spectra of reduced 7.5Ce-Ni-SBA catalyst in the Ni $2p_{1/2}$ core-level, Fig. 5 shows a large band centered at 855.0 eV that can be deconvoluted into three components. The first one at 852.8 eV is assigned to Ni^0; the low intensity of this band reveals that the reduction of nickel is not completely accomplished. However, the apparent low intensity of this band could be due to the fact that the photoelectron emerging from the core level of nickel are subsequently reabsorbed by other nickel atoms of the metallic particles. The peak at 855.0 eV reveals the presence of oxidized particles or unreduced NiO with high degree of interaction with ceria; while the more energetic signal at 857.5 eV could correspond to

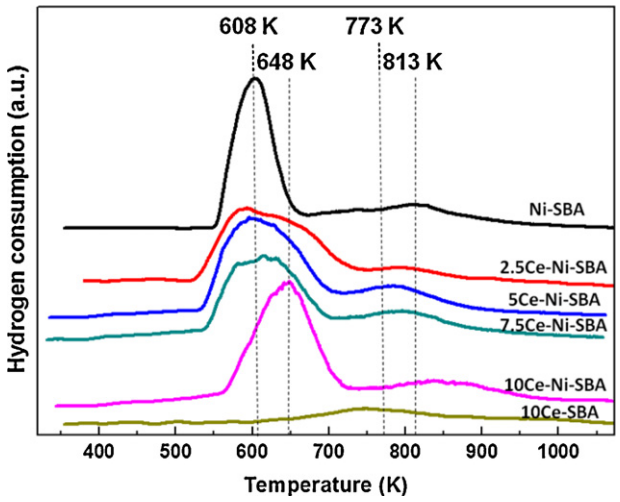

Fig. 3. H_2-TPR profiles of *X*Ce-Ni-SBA calcined catalysts, sample Ni free 10Ce-SBA was also included as reference.

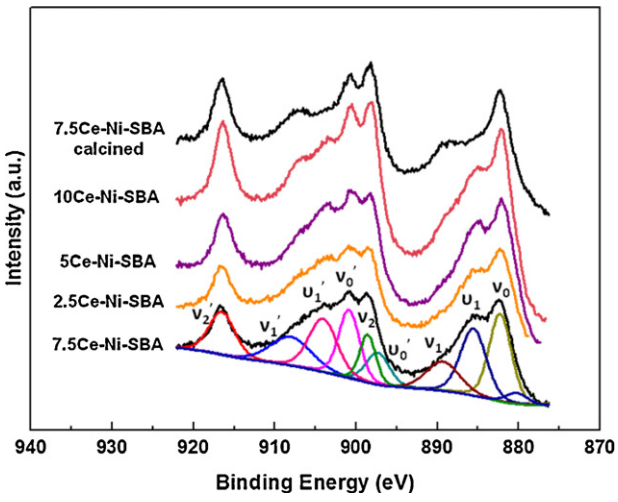

Fig. 4. Ce 3d photoelectron profiles of 7.5Ce-Ni-SBA calcined sample and CeNi reduced catalysts.

Table 3
Binding energies of cerium species and percentage of Ce(III) on the surface of CeNi reduced catalysts obtained by XPS.

Sample	Binding energy (eV)										Ce(III)(%)
	Calcined sample										
	Ce(IV)						Ce(III)				
	ν_0	ν_1	ν_2	ν'_0	ν'_1	ν'_2	υ_0	υ_1	υ'_0	υ'_1	
7.5Ce-Ni-SBA[a]	882.2	888.8	898.0	900.8	906.9	916.5	–	885.7	–	903.2	9.9
Sample	Binding energy (eV)										Ce(III)(%)
	Reduced catalysts										
	Ce(IV)						Ce(III)				
	ν_0	ν_1	ν_2	ν'_0	ν'_1	ν'_2	υ_0	υ_1	υ'_0	υ'_1	
2.5Ce-Ni-SBA	882.1	888.3	898.5	900.8	907.3	916.4	880.4	885.3	897.3	903.7	34.0
5.0Ce-Ni-SBA	881.9	888.9	898.1	900.5	907.4	916.2	880.3	885.3	897.3	903.7	35.3
7.5Ce-Ni-SBA	882.3	889.3	898.6	900.9	908.1	916.5	880.1	885.6	897.3	904.3	35.6
10Ce-Ni-SBA	881.9	887.4	898.2	900.4	906.6	916.3	880.2	885.0	898.0	902.7	27.4

[a] Calcined sample.

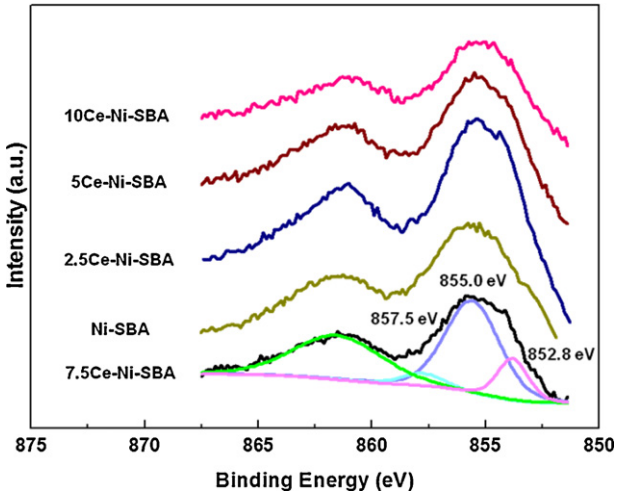

Fig. 5. Ni 2p core level spectrum for *X*Ce-Ni-SBA reduced catalysts.

either Ni^{2+} ions or very small NiO particles located on the walls of mesopores, as has been previously reported [39].

The Ni/Si atomic ratios for the different catalysts (Table 4) are almost constant owing to all them contain the same loading of nickel; however the Ce/Si atomic ratios increase along of this set of catalysts with the cerium content. Similar trend is observed for Ce/Ni atomic ratios but the corresponding values are lower than the nominal ones. This fact can be due to the low detection of Ni^0 with this technique as it has been commented above and possibly due to cerium ions are covering the nickel particles.

The total superficial acidity of the reduced catalysts was determined by NH_3-TPD between 373 and 823 K (Table 1). The total acidity of Ni-SBA reduced catalyst is much higher than that of the support (64 μmol NH_3 g^{-1}); the high increase of the total acidity is therefore due to the presence of the remaining Ni^{2+} ions are active as Lewis acid sites. The NH_3-TPD profile of this catalyst shows a peak at 430 K followed of a long tail till 750 K, due to the presence of more acidic sites (Fig. 6). When cerium species are incorporated to the catalysts, a new peak appeared at 615–623 K in the NH_3-TPD profiles; except for the 10Ce-Ni-SBA catalyst this second peak has increased intensity across the group when the loading of cerium is higher. Thus it is possible to conclude that this second peak is originated by the presence of cerium species. On the other hand, the higher the cerium content the higher the total acidity, reaching the maximum value for 7.5Ce-Ni-SBA catalyst with 1175 μmol NH_3 g^{-1}. This catalyst exhibited the lower degree of reduction of Ni^{2+} (Table 2), thus having the maximum concentration of this ion, and at the same time has the maximum degree of reduction of Ce(IV) to Ce(III), therefore is the most acidic sample. Moreover, this sample has the highest concentration of strong acid sites, i.e. the number of ammonia molecules desorbed between 573 and 823 K (Table 1).

Table 4
Atomic ratios of CeNi reduced catalysts obtained from XPS analysis.

Catalyst	Atomic ratios			Nominal atomic ratios
	Ce/Si	Ni/Si	Ce/Ni	Ce/Ni
2.5Ce-Ni-SBA	0.07	0.18	0.39	0.11
5Ce-Ni-SBA	0.12	0.16	0.67	0.21
7.5Ce-Ni-SBA	0.16	0.16	0.76	0.31
10Ce-Ni-SBA	0.21	0.14	1.46	0.42
Ni-SBA		0.16		

3.2. Catalytic activity

The hydrogenolysis of glycerol was performed for the different NiCe catalysts supported on mesoporous silica SBA-15 samples, previously reduced at 723 K under H_2 flow during 1 h (see Fig. 7). In all cases the concentration of the aqueous solution of glycerol used

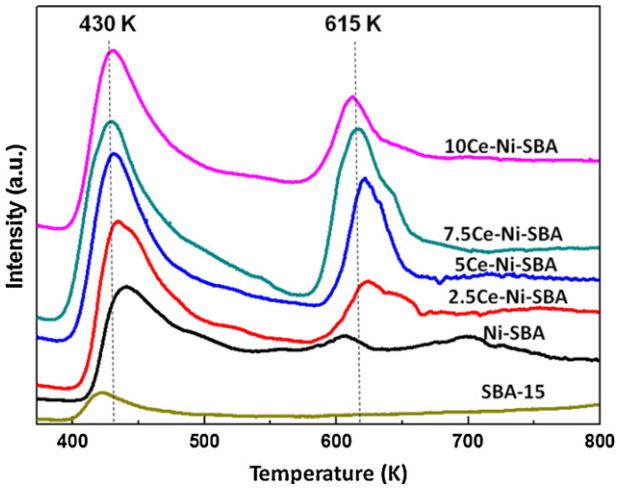

Fig. 6. NH_3-TPD profiles of *X*Ce-Ni-SBA reduced catalysts.

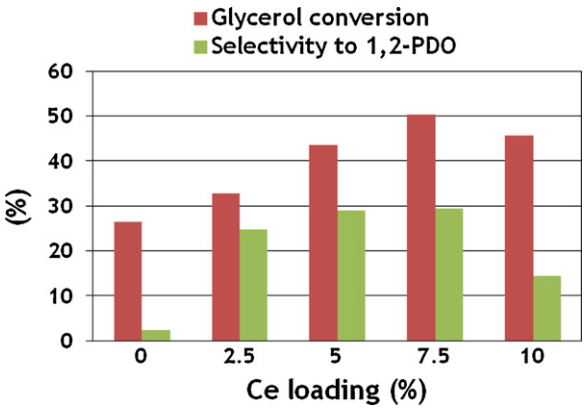

Fig. 7. Glycerol conversion and selectivity to 1,2-PDO of CeNi reduced catalysts versus cerium content. Reaction conditions: T = 473 K, P = 2.4 MPa, catalyst = 0.6 g, glycerol in water = 80 wt.%, reaction time = 8 h and stirring rate = 500 rpm.

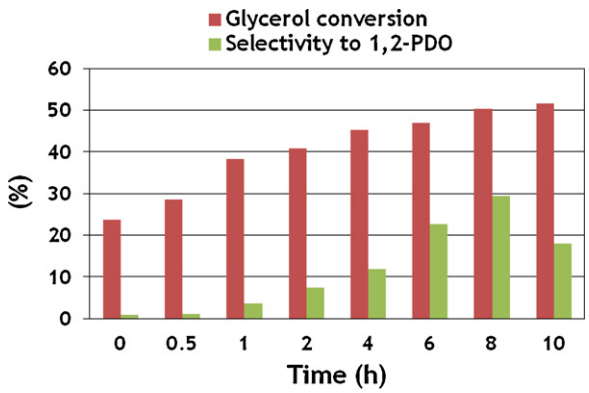

Fig. 8. Glycerol conversion and selectivity to 1,2-PDO of 7.5Ce-Ni-SBA reduced catalyst as a function of the reaction time. Reaction conditions were as in Fig. 7.

in the experiments was 80 wt.%, i.e. the same concentration that is obtained in the industrial transesterification of triglycerides under alkaline homogeneous reaction.

As a first step, the Ni-SBA was assayed in the experimental conditions described in Section 2, 2.4 MPa of H_2 and 473 K. After 8 h of reaction the found conversion of glycerol is high (26%), but the formation of 1,2-PDO is negligible, instead high concentrations of methanol, ethanol and volatile compounds were attained. This result means that a high cleavage of C—C bonds takes place on the Ni metallic particles. This is in agreement with the fact that metallic Ni at high temperatures is an active catalyst for methanation [43], as has been also found for the system Ni/Al_2O_3 [30]. On the other hand, taking into account that the metallic active phase is supported on a non-acidic solid, as is SBA-15 silica, the acetol route proposed for this reaction [28] cannot be expected.

When cerium is incorporated to the catalysts as a promoter, with loadings from 2.5 wt.% to 7.5 wt.%, and maintaining the nickel loading not only the conversion is enhanced, been maximum for the 7.5Ce-Ni-SBA catalyst with 51% of glycerol conversion, but the selectivity of the reaction is deeply modified (Fig. 7). For all promoted catalysts, mostly 1,2-PDO and also acetol were the predominant reaction products, although minor concentrations of ethylene glycol (selectivity lower than 2%) and traces of ethanol and methanol were also detected. We note that a fraction of reaction products cannot be identified and quantified by GC. Yet, we have dedicated important efforts to shed some light about the possible structure of these unidentified products. To do so, we have determined the H_2O concentration in the final reaction liquid by Karl Fisher titration. We found that this H_2O concentration after reaction was higher than expected considering the H_2O molecules released during glycerol dehydration reactions to form 1,2-PDO and acetol. The excess of H_2O may be due to glycerol condensation reactions to yield polyglycerols and/or to secondary dehydration reactions resulting in the formation of heavy products, undetectable by GC.

The 7.5Ce-Ni-SBA catalyst gives 29% of selectivity toward this compound, which is also the maximum selectivity among this group of catalysts. The results indicated that the incorporation of cerium to Ni-SBA material has an excellent promoting effect in this reaction owing to the presence of Ce(III) or Ce(IV) ions, which can act as strong acidic sites where the glycerol molecules can suffer in a first step a dehydration reaction. Since the ceria particles are interacting with nickel particles, as was deduced from the H_2-TPR studies, or at least they are located in their vicinity, the intermediate acetol is reduced in a second step with hydrogen activated on the metallic nickel particles. Increasing the cerium loading up to 10 wt.% in the catalyst, a reduction in both the conversion and selectivity of 1,2-PDO found, with values of 46% and 15%, respectively. The found results match well with the percentage of Ce(III) in the samples, as deduced from XPS analysis of the catalysts. Therefore, Ce7.5-Ni-SBA catalysts with the highest percentage of Ce(III) exhibits maximum conversion; taking into account that CeO_2 and Ce_2O_3 have the same crystalline fluorite structure, although in the last case a quarter of the oxygen anions is removed, therefore the formation of superficial Ce(III) on the ceria particles implies the existence of oxygen vacancies which can act as acid sites leading to a higher catalytic activity. In fact this catalyst exhibits not only the maximum content of acid sites, as was deduced from NH_3-TPD, but also the highest concentration of the strong acid sites, as is observed in Table 1. On the other hand, this catalyst shows also the highest metallic surface; thus, the number of H_2 molecules activated on these metallic sites is higher and can reduced in a great extend the acetol molecules formed in the acidic centeres. To consider the stability of the catalysts in the reaction conditions, the spent catalysts were studied by XRD and XPS analysis. The obtained results indicate that the particle sizes of metallic nickel of spent catalysts are very similar to those of fresh ones, which reveals that no sintering of the metallic particle takes place during the catalytic reaction. On the other hand, the XPS spectra in the Ni 2p region of spent samples are very close to those of fresh catalysts. All these data indicate that the catalysts are stable in the experimental conditions of the catalytic reaction.

It is noteworthy that the catalytic results found in this work are interesting and are similar [31] or even better than some previously reported in literature [33]. Thus, the yield of 1,2-PDO/g of catalyst is for the 7.5Ce-Ni-SBA sample of 24.2 under mild reaction conditions, higher than the values reported by Yu et al. [34,35], in spite of the concentration of glycerol used in the present work was very high (80 wt.%) and the H_2 pressure employed was lower. Nonetheless, Zhao et al. [30] obtained higher yield of 1,2-PDO per gram of catalyst when Ni was supported on an acid support as is NaX zeolite, but under higher pressures (6 MPa) and using diluted glycerol aqueous solutions (25 wt.%).

However, the experimental results obtained with Ce/Ni supported on SBA-15 silica are far from those obtained with noble metals (Pt and Pd/Cu) supported on solid-base catalysts [44,45]. These differences can be justified considering that the glycerol hydrogenolysis proceeds via a distinct mechanism of reaction on these solid-base catalysts, where in a first step glycerol is dehydrogenated to glyceraldehyde, followed by dehydration to 2-hydroxyacrolein and ulterior hydrogenation [16]. However, nickel catalysts present the advantage to be cheaper than those based on noble metals.

Concerning the exploration of the reaction conditions for the best catalyst 7.5Ce-Ni-SBA the reaction time and H_2 pressure were studied. Fig. 8 shows the influence of the reaction time on the

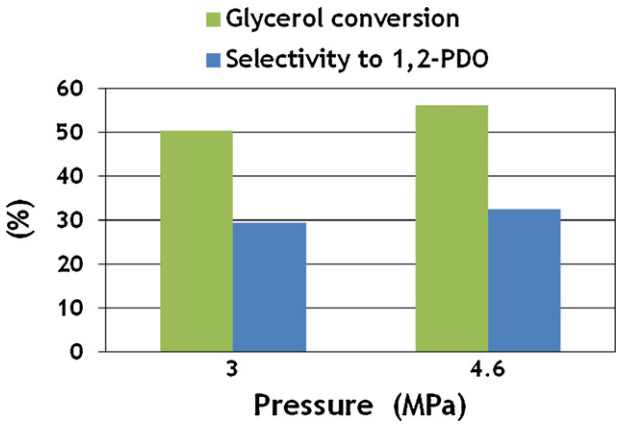

Fig. 9. Influence of the pressure on the glycerol hydrogenolysis of the 7.5Ce-Ni-SBA catalysts. The rest of reaction conditions were the same as in Fig. 7.

glycerol conversion and on 1,2-PDO selectivity. Up to 8 h of the reaction time both the conversion and the formation of 1,2-PDO monotonically increased, although an ulterior increment in the reaction time (10 h) still leads to an slightly increase in the glycerol conversion, on the contrary a longer time of reaction originated low selectivity of 1,2-PDO due to its partial decomposition. Finally, the effect of the hydrogen pressure was investigated varying the total pressure. Fig. 9 shows that increasing the pressure from 3 to 4.6 MPa the conversion was slightly enhanced till 56% as well as the selectivity that raised up to 32.5%. However, a low pressure of H_2 as 3 MPa is recommended, because that implies milder reaction conditions.

4. Conclusions

Nickel supported on SBA-15 catalysts promoted with cerium, loading varying from 2.5 to 10 wt.%, are active in the hydrogenolysis reaction of glycerol to produce 1,2-PDO. Since Ni-SBA catalyst is practically inactive in the formation of such product because mainly volatile compounds are formed by C—C cleavage reaction, the presence of cerium species, which provide higher surface acidity, leads to the formation of intermediate acetol which is later reduced by H_2 coming from Ni metallic sites. The catalyst 7.5Ce-Ni-SBA is the most active in the mild conditions, since this catalyst have the maximum concentration of acid sites formed during the reduction of the catalysts at 723 K under H_2, attaining 24.2% of yield of 1,2-PDO per gram of catalyst after 8 h of reaction and under mild reaction conditions.

Acknowledgments

The authors are grateful to financial support from the Spanish Ministry of Science and Innovation (ENE2009-12743-C04-03/01 projects) and Junta de Andalucía (P09-FQM-5070) and FEDER funds. IJM would like to thank the Agencia Estatal of CSIC for a JAE-Predoctoral grant (Research Training, JAE Programme) and for a stage in ICP of CSIC.

References

[1] A. Dermibas, Energy Sources, Part A, Taylor & Francis Group, L.L.C., 2009, pp. 1770–1776.
[2] S. Fernando, S. Adhikari, C. Chandapral, N. Murali, Energy Fuels 20 (2006) 1727–1737.
[3] C.H. Zhou, J.N. Beltramini, Y.X. Fan, G.Q. Lu, Chem. Soc. Rev. 27 (2008) 527–549.
[4] R.R. Soares, D.A. Simonetti, J.A. Dumesc, Angew. Chem. Int. Ed. 45 (2006) 3982–3985.
[5] T. Hirai, N. Ikenega, T. Miyake, T. Suzuki, Energy Fuels 19 (2005) 1761–1762.
[6] I. Furikado, T. Miyazawa, S. Koso, A. Shimao, K. Kunimori, K. Tomishige, Green Chem. 9 (2007) 582–588.
[7] T. Haas, B. Jaeger, R. Weber, S.F. Mitchell, Appl. Catal. A: Gen. 280 (2005) 83–88.
[8] E. Watanabe, T. Lida, Y. Aizawa, T.M. Alda, H. Inomata, Bioresour. Technol. 98 (2007) 1285–1290.
[9] E. Tsukuda, S. Sato, R. Takanashi, T. Sodesawa, Catal. Commun. 8 (2007) 1349–1353.
[10] S. Demiral, K. Lehnert, M. Lucas, P. Claus, Appl. Catal. B 70 (2007) 637–643.
[11] Y. Amada, Y. Shinmi, S. Koso, T. Kubota, Y. Nakagawa, K. Tomishige, Appl. Catal. B: Environ. 105 (2011) 117–127.
[12] Y. Nakagawa, Y. Shinmi, S. Koso, K. Tomishige, J. Catal. 272 (2010) 191–194.
[13] Y. Shimi, S. Koso, T. Kubota, Y. Nakagawa, K. Tomishige, Appl. Catal. B: Environ. 94 (2010) 318–326.
[14] S. Wang, H. Liu, Catal. Lett. 117 (2007) 62–67.
[15] A. Alhanash, E.F. Kozhevnikova, I.V. Kozhenikov, Catal. Lett. 120 (2008) 307–311.
[16] C. Montassier, J.C. Ménézo, L.C. Hoang, C. Ranaud, J. Barbier, J. Mol. Catal. 70 (1991) 99–110.
[17] T. Miyazawa, S. Koso, K. Kunimori, K. Tomishige, Appl. Catal. A 318 (2007) 244–251.
[18] T. Miyazawa, Y. Kusonoki, K. Kunimori, K. Tomishige, J. Catal. 240 (2006) 213–221.
[19] T. Miyazawa, S. Koso, K. Kunimori, K. Tomishige, Appl. Catal. A 329 (2007) 30–35.
[20] J. Feng, H. Fu, J. Wang, R. Li, H. hen, X. Li, Catal. Commun. 9 (2008) 1458–1464.
[21] M. Balaraju, V. Rehka, B.L.A.P. Devi, R.B.N. Prasad, P.S.S. Prasad, N. Lingaiah, Appl. Catal. A 383 (2010) 107–114.
[22] E.P. Maris, R.J. Davis, J. Catal. 249 (2007) 328–337.
[23] D.G. Lahr, H. Shanks, J. Catal. 232 (2005) 386–394.
[24] E.P. Maris, W.C. Ketchie, M. Murayama, R. Davis, J. Catal. 251 (2007) 281–294.
[25] L. Ma, H. De, Top. Catal. 52 (2009) 834–844.
[26] J.N. Chheda, G.W. Huber, J.A. Dumesic, Angew. Chem. Int. Ed. 46 (2007) 7164–7183.
[27] E.P. Maris, W.C. Ketchie, M. Murayama, R.J. Davis, J. Catal. 251 (2007) 281–294.
[28] A. Perosa, P. Tundo, Ind. Eng. Chem. Res. 44 (2005) 8535–8537.
[29] Y. Kusunoki, T. Miyazawa, K. Kunimori, K. Tomishige, Catal. Commun. 6 (2005) 645–649.
[30] J. Zhao, W. Yu, C. Chen, H. Miao, H. Ma, J. Xu, Catal. Lett. 134 (2010) 184–189.
[31] M.A. Dasari, P.P. Kiatsimkul, W.R. Sutterlin, G.J. Suppes, Appl. Catal. A 281 (2005) 225–231.
[32] A. Marinoiu, G. Ionita, C.L. Gáspár, C. Cobzaru, D. Marinescu, C. Teodorecu, S. Oprea, React. Kinet. Mechan. Catal. 99 (2010) 111–118.
[33] L. Huang, Y.L. Zhu, H.Y. Zheng, Y.W. Li, Z.Y. Zeng, J. Chem. Technol. Biotechnol. 83 (2008) 1670–1675.
[34] W. Yu, J. Xu, H. Ma, Ch. Chen, J. Zhao, H. Miao, Q. Song, Catal. Commun. 11 (2010) 493–497.
[35] W. Yu, J. Zhao, H. Ma, H. Miao, Q. Song, J. Xu, Appl. Catal. A 383 (2010) 73–78.
[36] H.X. Li, S.H. Zhang, H.S. Luo, Mater. Lett. 58 (2004) 2741–2746.
[37] M. Gómez-Cazalilla, J.M. Mérida-Robles, A. Gurbani, E. Rodríguez-Castellón, A. Jiménez-López, J. Solid State Chem. 180 (2007) 1130–1140.
[38] D.J. Lensveld, J.G. Mesu, A. Jos van Dillen, K.P. de Jong, Micopor. Mesopor. Mater. 44–45 (2001) 401–407.
[39] D. Eliche-Quesada, J. Mérida-Robles, P. Maireles-Torres, E. Rodríguez-Castellón, A. Jiménez-López, Langmuir 19 (2003) 4985–4991.
[40] J.W.E. Coenen, Appl. Catal. 75 (1991) 193–223.
[41] L. Qiu, F. Liu, L. Zhao, Y. Ma, J. Yao, Appl. Surf. Sci. 252 (2006) 4931–4935.
[42] F. Zhang, P. Wang, J. Koberstein, S. Khalid, S.W. Chan, Surf. Sci. 563 (2004) 74–82.
[43] Y.L. Zhu, G.W. Zhao, J. Chang, J. Yang, H.Y. Zheng, H.W. Xiang, Y.-W. Li, Catal. Lett. 96 (2004) 123–127.
[44] Z. Yuan, P. Wu, J. Gao, X. Lu, Z. Hou, X. Zheng, Catal. Lett. 130 (2009) 261–265.
[45] S. Xia, Z. Yuan, L. Wang, P. Chen, Z. Hou, Appl. Catal. A: Gen. 403 (2011) 173–182.